ELSEVIER

Cement and Concrete Composites **18** (1996) 125–133

0958-9465/96/$15.00

PII:S0958-9465(96)00009-1

Model for Predicting the Fracture Process Zone and *R*-curve for High Strength FRC

A.-B. Eissa[a] & G. Batson[b]

[a]GPC, ICS Department, Doha, Qatar
[b]Professor, Civil and Environmental Engineering Department, Clarkson University, Potsdam, NY 13699, USA

Abstract

An analytical model based on the weight function method is used to assess the toughness of high strength steel fiber reinforced concrete notch beams for different fiber types and fiber volume percentages. The crack mouth opening displacement, CMOD, the crack tip opening displacement, CTOD and the J-intergral are obtained by an iterative procedure to similate the experimental load–CMOD response of the beams. Copyright © 1996 Elsevier Science Ltd.

Keywords: Weight function, CMOD, CTOD, *R*-curve, steel fiber reinforced concrete, toughness.

INTRODUCTION

It is generally accepted that fracture toughness of fiber reinforced concrete cannot be evaluated using linear elastic fracture mechanics (LEFM) without modifications because of a nonlinear zone ahead of the crack tip often termed the fracture process zone. The nonlinearity of the process zone arises from heterogeneity inherent in concrete, microcracking ahead of the crack tip, and from fiber bridging in fiber reinforced concrete. The presence and the important influence of the fracture process zone in concrete has been recognized since the late 1970s.[1]

Fracture mechanics models often simulate the bridging effect of fibers with a closing pressure on the crack surface. Hillerborg extended his fictitious crack model to fiber reinforced concrete by proposing that the closing pressure to be a function of fiber length, fiber diameter and interface bond strength.[1] Visalvanich and Naaman developed a similar model using a closing pressure that depends on a 'fiber efficiency factor' and is a power function of the crack profile.[2] Wecharatana and Shah assumed a parabolic closing pressure for fiber toughening.[3] Balaguru *et al.* proposed a model to predict matrix toughening in fiber reinforced concrete.[4] Jenq and Shah proposed a two parameter fracture model to establish a criteria for unstable crack propagation.[5] Li and Liang proposed a numerical model for the prediction of the fracture process zone for concrete and fiber reinforced concrete.[6] Several approaches to the study of the fracture of cementitious materials have been proposed recently. These approaches can be categorized as either cohesive crack models or effective crack models. In cohesive crack models, the fracture process zone is modeled by applying traction forces across the surfaces of newly formed cracks. The first application of cohesive crack models to concrete was by Hillerborg *et al.*[7] Since then the cohesive crack model has been successfully applied to the study of concrete failure.[8] A basic requirement of the cohesive crack model is the softening curve, sometimes known as the 'stress–separation curve', which relates the stresses across the crack surfaces, the cohesive stresses, to the corresponding crack openings.

Guinea *et al.* [9] reported that a bilinear softening curve suffices to characterize the softening behavior of concrete. However, Guinea *et al.* [9] argued that in many practical situations knowledge of the whole softening curve is not needed and only the initial slope of the softening curve matters. For a very large specimen size the whole curve is required, whereas for a very small specimen size only the initial slope of the softening curve matters and the tail of the curve is irrelevant. They defined

a characteristic length for concrete as $D_c = 0.9\ell_{ch}$, where ℓ_{ch} is Hillerborg's characteristic length. When the size of the specimen is less than D_c the tail of the softening curve is irrelevant because at this size, the specimen behaves as a material with a linear softening curve. Guinea *et al.* [9] showed that plain concrete has a standard value of 300 mm for ℓ_{ch} and $D_c = 270$ mm. For fiber reinforced concrete the value of ℓ_{ch} is between 2–20 m which gives a much larger value for D_c.

The test specimens in this project are small size specimens, $152 \times 229 \times 686$ mm ($6 \times 9 \times 27$ in) with a notch 57 mm (2.25 in) deep. The notched beams were tested in four bending using a closed loop crack-mouth-opening-dispalcement (CMOD) controlled testing machine. A data acquisition recorded the load and output of the CMOD compliance gage. Tables 1, 2 and 3 provide a summary of the concrete mixture proportions, compressive strength and fiber properties.

Based on the above reasoning, a linear stress–separation curve was assumed to model the fiber bridging effect for the cohesive crack model. The model uses the weight function method and an iterative procedure to match the experimentally obtained load vs CMOD curves. The model simulates the behavior of the fracture process zone as well as the length traction free crack. The model also allows the calculations of the crack tip opening displacement, CTOD, and the J-integral at any load level. The J-integral values at selected load points are plotted against the calculated traction free crack to produce the crack resistance curves, R-curves.

Mai [10] suggested that the fracture behavior of fiber cementitious composites can be described adequately by R-curves. The R-curve, which is material, geometry, and size-dependent, is a convenient means of studying the crack growth and the toughening effects of fibers. In this research, the R-curve approach is used to predict the toughness effects of two different fiber types and three different fiber volume percentages. It should be noted that the calculated values of the R-curves and the J-integral values

Table 1. High strength FRC mixture

Type III Cement	1420 kg/m^3 (850 lb/yd^3)
Silica Fume	20%
Fly Ash	15%
W/CC+SF+FA)	0.22
9 mm (3/8 inch) stone	2086 kg/m^3 (1680 lb/yd^3)
Sand	1511 kg/m^3 (905 lb/yd^3)
HRWA	23 liters (780 fl. oz/yd^3)

Table 2. Average compressive strength

Age (day)	*fc'*	*(Average of 30 tests)*
7	66.9 MPa	(9710 psi)
14	74.9 MPa	(10870 psi)
28	90.9 MPa	(13210 psi)
56	108.9 MPa	(15800 psi)

Table 3. Properites of fibers

Fiber type	*Fiber length*	*Diameter (in)*	*Aspect ratio (l/d)*	*Volume fraction %*
Hooked-end	50 mm (2 in)	0.50 mm (0.02 in)	100	0.5,1.0,1.5
Crimped	50 mm (2 in)	1 mm (0.04 in)	50	0.5,1.0.1.5

at the peak load, J_{peak}, are calculated based on the simplifying assumption that the traction free crack growth starts at the maximum load. This assumption seems to be very common in the literature on fracture mechanics of concrete and fiber reinforced concrete because of the difficulty in identifying the exact location of the crack tip in cementitious materials and it has been adopted by several researchers.[10,3,11,12]

WEIGHT FUNCTION METHOD

The weight function method was first introduced by Büeckner.[13] Rice [14] followed by showing that the weight function is a universal function for a cracked body of any given geometry and composition, regardless of the detailed way in which the body is loaded. One particular feature of the weight function method is the remarkable computational efficiency achieved without compromising the solution accuracy. The concept of the weight function permits the determination of the stress intensity factor for any applied stress distribution $\Sigma(X)$ in the body, if the crack opening displacement $U_r(A,X)$ and the related stress intensity factor $K_r(A)$ of a reference load case are known for the geometry of the body. The stress intensity factor is given by:

$$K(\mathrm{A}) = \frac{\mathrm{E}'}{K_r(A)} \int_0^A \Sigma(\mathrm{X}) \frac{\partial U_r}{\partial A}(A,X)\, \mathrm{d}X \tag{1}$$

where $E' = E$ for plane stress, $E' = E/1-\upsilon^2)$ for plane strain, A = the crack length and the coordinate X coincides with the crack line with its origin at the crack mouth as shown in Fig. 1.

It is advantageous from the computational point of view to write this equation in a non-dimensional form. For this purpose, a normalizing stress, σ, which can be taken as the far field stress and a characteristic dimension, W, are introduced. In addition, the following non-dimensional terms are defined:

$$l = \frac{L}{W},\ x = \frac{X}{W},\ a = \frac{A}{W},$$

$$u_r(a,x) = \frac{U_r(A,X)}{W} \tag{2}$$

Thus,

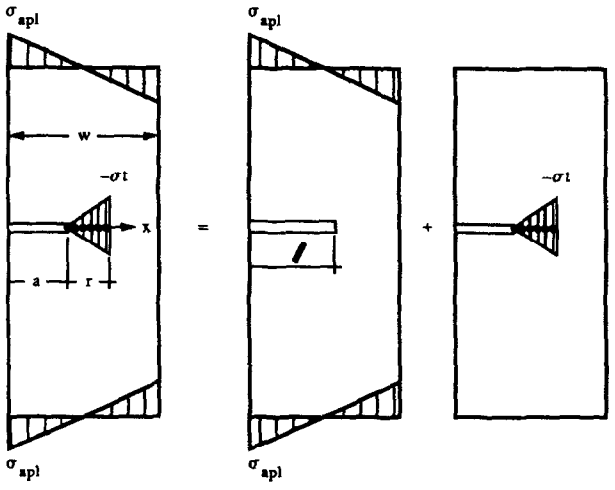

Fig. 1. Superposition of the problem.

$$\frac{K(A)}{\sqrt{W}} = \int_0^a \sigma(x) h_r(a,x)\, dx \tag{3}$$

or

$$K(A) = f(a)\sigma\sqrt{\pi a W} \tag{4}$$

where

$$f(a) = \int_0^a \frac{\sigma(x) h_r(a,x)}{\sigma\sqrt{\pi a}}\, dx \tag{5}$$

in which $h_r(a,x)$ is the weight function given by

$$h_r(a,x) = \frac{E'}{f_r(a)\sigma\sqrt{\pi a}} \frac{\partial u_r(a,x)}{\partial a} \tag{6}$$

where

$$f_r(a) = \frac{K_r(A)}{\sigma\sqrt{\pi a}} \tag{7}$$

CRACK OPENING DISPLACEMENTS

Knowledge of crack opening displacements is essential for stable crack growth analysis, modeling of material toughening, residual stress effect assessment, and in experiments to determine crack length using compliance methods. The weight function method provides a powerful and efficient means for the determination of crack opening displacements. The evaluation of crack opening displacements using the weight function depends on the crack-line load distribution assumed. If the crack face loading is

continuous, the displacement can be calculated based on an analytical representation for the crack opening displacement. In a more general method, the crack opening displacement can be calculated by the integration of the product of a stress intensity factor and a weight function.

Direct calculation based on the crack opening displacement equations

Wu and Carlsson [15] have proposed the following normalized reference crack face displacement representation by combining William's series expression and the Petroski and Achenbach [16] approach:

$$U_r(a,x) = \frac{\sigma}{\sqrt{2}} \frac{a}{E'} \sum_{j=1}^{4} F_j(a) \left(1 - \frac{x}{a}\right)^{j-1/2},$$

$$0 \le \frac{x}{a} \le 1 \tag{8}$$

where the $F_j(a)$ functions are determined by the following four conditions: The first term in the expansion of eqn (8) dominates in the crack-tip region.

Self-consistency requires the recovery of the reference stress intensity factor when the derived weight function is applied back to the reference load case itself.

Curvature of an edge crack vanishes at the crack mouth.

The CMOD at the crack mouth is known.

Integration of the product of stress intensity factor and weight function

A more general way to determine crack opening displacement for arbitrary crack-line loadings is to use the relationship between the weight function $h(a,x)$ and the crack surface displacement $u(a,x)$:[15]

$$\frac{E'}{K(A)} \frac{\partial U(A,X)}{\partial A} = \frac{E'}{K_r(A)} \frac{\partial U_r(A,X)}{\partial A} \tag{9}$$

Equation (9) can be written in a non-dimensional form as follows:

$$\frac{E'}{f(a)\sigma\sqrt{\pi a}} \frac{\partial u(a,x)}{\partial a} = h_r(a,x) \tag{10}$$

Integrating both sides of eqns (9) and (10) and rearranging leads to the following equation for the crack opening displacement:

$$u(a,x) = \frac{\sigma}{E'} \int_{a_0}^{a} [f(s)\sqrt{\pi s}] h_r(s,x)\, ds \tag{11}$$

where $a_o = \max(a,x)$ and s is a dummy variable.

THE WEIGHT FUNCTION

A closed form weight function is readily determined by partial differentiation of the displacement function eqn (8) with respect to the crack length, a: [15]

$$h_r(a,x) = \frac{1}{\sqrt{2\pi a}} \sum_{i=1}^{J+1} \beta_i(a) \left(1 - \frac{x}{a}\right)^{i-3/2}, x \le a \tag{12}$$

where:

$$\beta_1(a) = 2.0$$

$$\beta_2(a) = (4af'_r(a) + 2f_r(a) + \frac{3}{2} F_2(a))/f_r(a)$$

$$\beta_3(a) = (aF'_2(a) + \frac{5}{2} F_3(a) - \frac{1}{2} F_2(a))/f_r(a)$$

$$\beta_4(a) = (aF'_3(a) + \frac{7}{2} F_4(a) - \frac{3}{2} F_3(a))/f_r(a)$$

$$\beta_5(a) = (aF'_4(a) - \frac{5}{2} F_4(a))/f_r(a) \tag{13}$$

and f_r is the normalized stress intensity factor for the reference load case. The appropriate F_j and f_r functions are based on the reference load case chosen.

PROBLEM FORMULATION AND SOLUTION TECHNIQUE

Referring to Fig. 1, the total crack length can be divided into two zones: a traction free length, a, and a fracture process zone length, r, in which the traction exists across the zone. If it is assumed that the stresses in the fracture pro-

cess zone are purely uniaxial, then it can be presented as a traction free length on which closing pressure exists. The closing pressure models the action of the fibers across the crack. A linear closing pressure distribution (a linear stress–separation relationship) is assumed with a value of zero at the physical crack tip (traction free crack tip) and a value equal to the tensile strength of the material, σ_t, at the notional crack tip (traction free crack length+fracture process zone length). The concept is somewhat similar to that proposed by Dugdale [17] and Barenblatt [18] for metals, and Hillerborg *et al.* [7] for normal strength-concrete.

The model solution can be obtained from the superposition of two elastic crack problems which are easily handled with the weight function method. In both problems, the crack geometry is the same but the load conditions are different, Fig. 1. In the first problem, the beam is loaded by a bending stress distribution $\sigma(x)$, of the form:

$$\frac{\sigma(x)}{\sigma_{apl}} = 1-2x \tag{14}$$

resulting from the applied stress σ_{apl}, while in the second problem, the fracture process zone is loaded by a linear stress distribution with a peak value equal to the tensile stress of the material, σ_t, at the notional crack tip and a value of zero at the physical crack tip. In Fig. 1, x is the normalized distance measured from the crack mouth, W is the total depth of the beam, a is the normalized traction free crack length, r is the normalized length of the fracture process zone, and ℓ is the normalized total crack length ($\ell = a+r$).

The crack opening displacement, COD, at any distance X along the crack surface can be obtained by superimposing the displacement U_{apl} (L,X), due to the applied load, and the displacement $U_t(L,X)$, due to the closing pressure. Thus the

$$\text{COD} = 2U(L,X) = 2[U_{apl}(L,X)+U_t(L,X)] \tag{15}$$

where $X=0$ for the crack mouth opening displacement, CMOD, and $X=A$ for the crack tip opening displacement, CTOD. All the required quantities in the above equation can be evaluated by using the weight function method.

The crack opening displacement, $U_{ap\ell}$, due to the external applied bending stress distribution can be found by using the stress intensity factor solution for pure bending and the crack mouth opening displacement Tada *et al.*[19] Details of the solution can be found in Eissa.[20] For the crack opening displacement, U_t, due to a linear closing pressure there is no readily available solution for the stress intensity factor and the crack opening displacement in the literature. An analytical equation for the stress intensity factor for the given closing pressure was derived using the weight function method. The analytical details can be found in Eissa.[20] The results for U_{apl} and U_t allow the COD of eqn (15) to be used for the calculation of either the CMOD or the CTOD.

Resistance curves, R-curves, were computed by plotting the J-integral vs the traction free crack length. The J-integral for straight crack faces is

$$J = \frac{\sigma_t(\text{CTOD})}{2} \tag{16}$$

where σ_t is the tensile strength of the steel fiber reinforced concrete. Solutions for the CMOD, CTOD and the J-integral were obtained by an iterative procedure. The traction free crack length and the fracture process zone length were incrementally increased, and each combination of traction free crack length and fracture process zone length were checked against the following constraints:

The fracture process zone length must satisfy the condition that the stress intensity factor due to the externally applied loading and the stress intensity factor due to the closing pressure cancelled one another at the notional crack tip.

The theoretically obtained CMOD did not vary from the experimentally obtained CMOD by more than 5%.

A check for interpenetration was carried out by rejecting any solution that gives a negative value for the CTOD.

CMOD was always greater than the CTOD.

No crack closing was allowed in the model, i.e. CTOD_{i+1} was always greater than CTOD_i as well as a_{i+1} was always greater than a_i.

Three assumptions were imposed on the solutions:

The length of the fracture process zone and the length of the traction free crack remained unchanged during the linear behavior of the material.

At the onset of the nonlinear behavior, the fracture process zone was allowed to increase

while keeping the traction free crack unchanged.

Once the peak load was reached, the traction free crack length and the fracture process zone were allowed to change.

The analytical results for each steel fiber reinforced concrete test beam consisted of graphs of the *R*-curve, fracture process zone length vs traction free crack length, the fracture process zone length vs time and the experimentally determined load vs CMOD. The graph of the fracture process zone length vs time could be computed because all the tests were conducted under displacement control and therefore the time from the start of the test for any load or CMOD during the test was known.

Figures 2(a), (b), (e) and (d) are the set of graphs for test beam A2-H-N-CM-1.5. The beam designation is:

A2 — beam number
H — hooked end fiber or C-crimped fiber
N — notched beam
CM — CMOD controlled test
1.5 — fiber volume percentage

Figures 3(a)–(d) summarize the results of one size of notched beam for two fiber types and two fiber volume percentages. Figure 3(a) is the *R*-curve for two different volume percentages of crimped fibers. The *R*-curve initially rises vertically, indicating no crack extension at low stress levels, but continues to rise with increasing traction free crack length. Because no plateau is reached in the *R*-curve, no critical crack growth has occurred. The increasing resistance to crack growth is primarily due to a progressive failure process in the fracture process zone. The fracture process includes fiber debonding and pull-out or fiber fracture as well as any inelastic deformation of the fibers. A visual examination of fractured surfaces of test specimens in the experimental program indicated fiber pull-out was the major failure mechanism although some fibers were observed

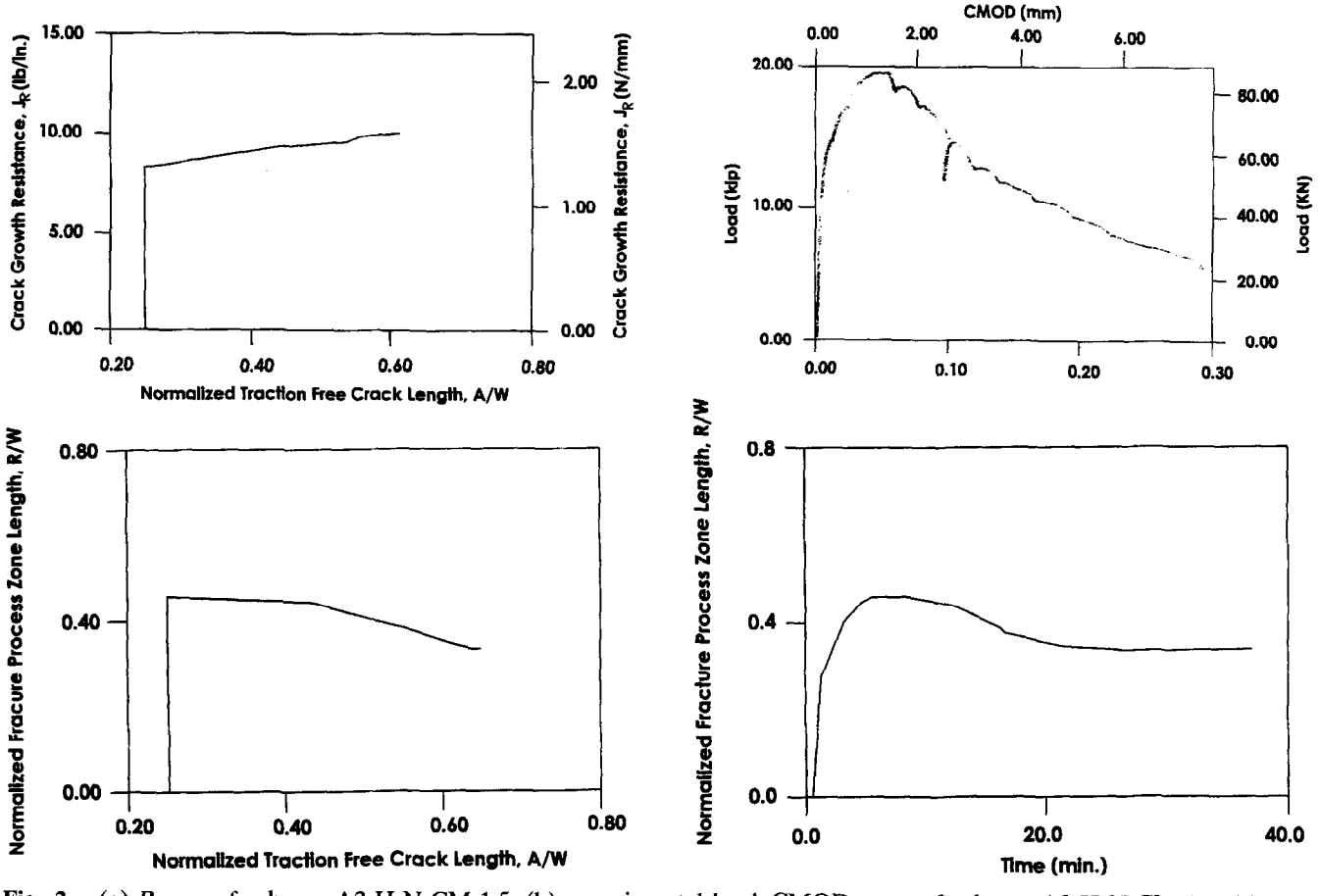

Fig. 2. (a) *R*-curve for beam A2-H-N-CM-1.5, (b) experimental load–CMOD curves for beam A2-H-N-CM-1.5, (c) FPZ length vs traction free crack length for beam A2-H-N-CM-1.5 and (d) FPZ length growth with time for beam A2-H-N-CM-1.5.

to be fractured. The general shape of the *R*-curves obtained in this research is comparable to those reported by Li *et al.*,[6] Wecharatana *et al.* [3] and Visalvanich *et al.*[2] for normal strength concrete reinforced with steel fibers. The value of J_{peak} for the beams analyzed in this study ranged from 0.7 N/mm to 1.4 N/mm. Swamy [21] stated that values of J_{peak} ranging from 0.04 N/mm to 3.85 N/mm have been reported by different researchers for steel fiber reinforced concrete. The enhancement in the matrix toughness due to an increase in fiber volume percentage is apparent in Fig. 3(a). Similar results were obtained for beams reinforced with hooked-end fibers.

Figure 3(b) shows different *R*-curves for the beams reinforced with two types of fibers and two different fiber volume percentages. Comparing the slopes of the second portion of the *R*-curves for the two fiber types, it can be seen that the slopes of the crimped fibers at 1.0 and 1.5 percent are steeper than those for hooked-end fibers at the same fiber volume percentages. This suggests that crimped fibers are superior to the hooked-end fibers at 1.0 and 1.5 volume percentages in enhancing the crack resistance and the toughness of a high-strength concrete matrix.

Comparing the values of J_{peak} calculated at the peak load, it is apparent that J_{peak} increases with an increase in fiber volume percentages, but there was no difference between the value of J_{peak} for crimped fibers and hooked-end fibers at 1.0% and only a marginal difference between the value of J_{peak} for both types of fibers at 1.5%. This suggests that J_{peak} values can be used to distinguish fiber performance based on fiber volume percentage but not fiber type. However, the entire *R*-curve may be reliable for distinguishing fiber performance based on both fiber type and fiber volume percentages.

Figure 3(c) shows the calculated values of crack tip opening displacements vs time for beams reinforced with crimped fibers. At a given time, beams with higher fiber volume percentage have higher values of CTOD indicating that more energy has been dissipated in beams

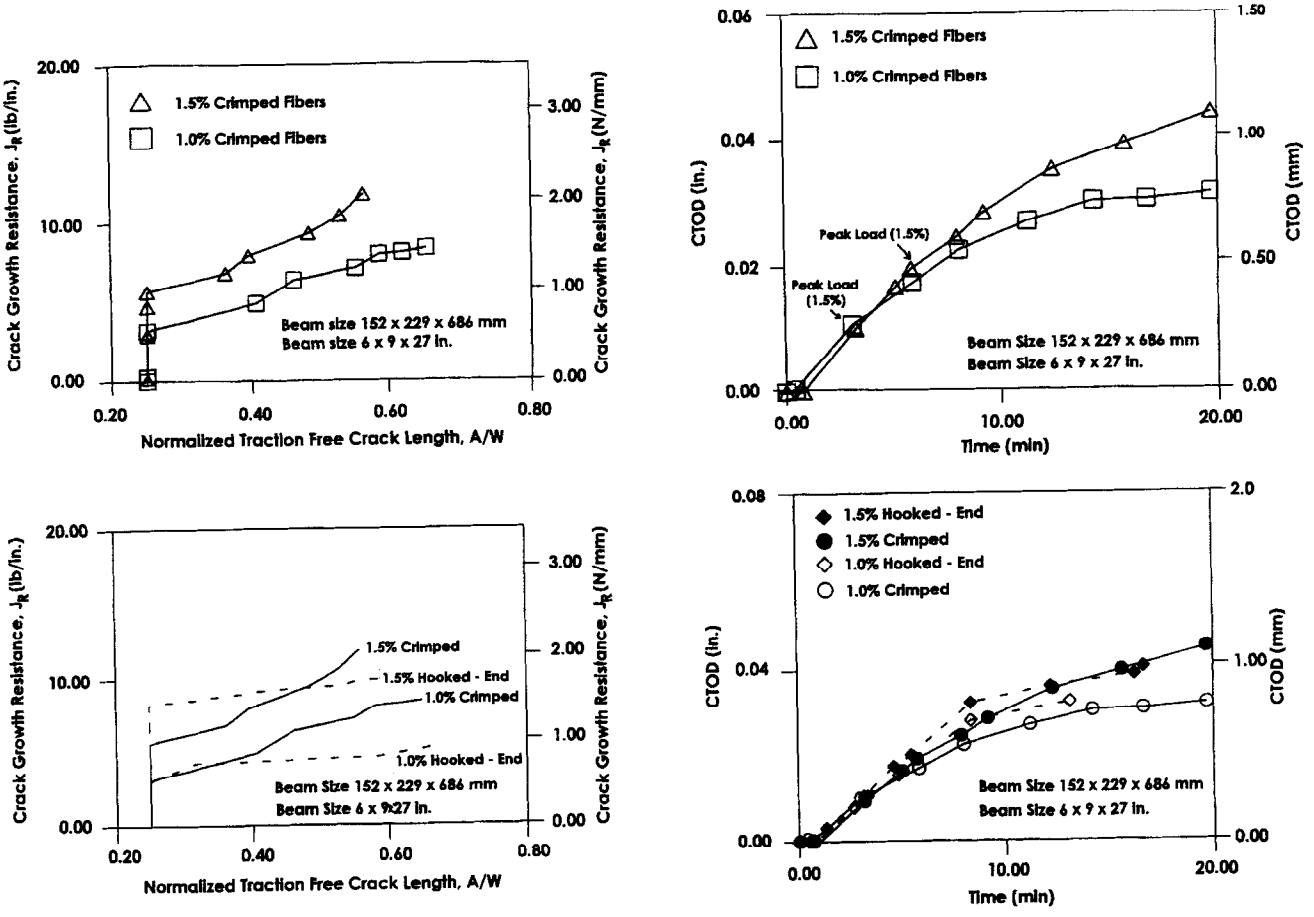

Fig. 3. (a) J_R for different fiber percentage, (b) CTOD vs time of different fiber percentage, (c) J_R for different fiber percentage and type and (d) CTOD vs time for different fiber percentage and type.

with higher fiber volume percentages. Figure 3(c) shows the same relationship as in Fig. 3(b) but in terms of fiber type. Initially the slopes of the lines representing the beams reinforced with crimped fibers and hooked-end fibers are almost the same, but then the lines representing the beams reinforced with hooked-end fibers show a decrease in slope with time. Beams reinforced with crimped fibers dissipate more energy than the hooked-end fibers and therefore exhibit increased toughness compared to beams reinforced with hooked-end fibers. Crimped fibers compared to hooked-end fibers are better for the toughening of the high-strength concrete matrix.

Figure 4 shows the computed load–CMOD curve generated by the iterative procedure outlined in the previous section. The computed values of the load and CMOD are connected by straight line segments. Figure 4 is in good agreement with Fig. 2(b), the experimentally obtained load–CMOD curve. The complete details of the experimental testing procedure can be found in Eissa.[20]

CONCLUSIONS

The non-linear fracture model based on a weight function method can be used to calculate *R*-curves and provide a comprehensive method for evaluating the fracture behavior of high strength steel fiber reinforced notched beams subjected to flexural loading.

Based on the test data and the method of analysis, the crimped fibers are more effective for increasing toughness because the crimped fibers dissipated more energy than an equivalent volume of hooked-end fibers.

The procedure is calculation intensive and may be impractical compared to either the standard ASTM C1018 [22] or JSCE-SF4 [23] for assessing the fracture toughness or to distinguish the differences in fracture toughness for various sizes, shapes or volume percentage of fibers.

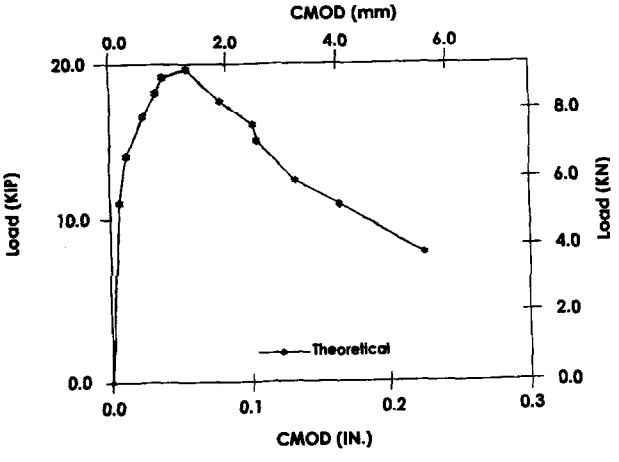

Fig. 4. Experimental and theoretical load–CMOD curves beam A2-H-N-CM-1.5.

ACKNOWLEDGEMENTS

The authors would like to thank the National Science Foundation (Structures, Geomechanics and Building Systems, Director Dr. Ken Chong, Grant No. 8906940) for financial support of this project.The theoretical model based on the weight function method was suggested by Dr. John Dempsey, CEE Department, Clarkson University and his continuous advice and guidance is greatly appreciated by Drs Eissa and Batson.

REFERENCES

1. Hillerborg, A., Modeer, M. & Patersson, P. E., Analysis of crack formation and crack growth in concrte by means of fracture mechanics and finite elements. *Cement and Concrete Research*, **6** (1976) 773–782.
2. Visalvanich, K. & Naaman, A. E., Fracture model for fiber reinforced concrete. *ACI Journal*, **80** (1983) 128–138.
3. Wecharatana, M. & Shah, S. P., A model for predicting fracture resistance of fiber reinforced concrete. *Cement and Concrete Research*, 13 (1983) 819–829.
4. Balaguru, P., Narahari, R. & Patel, M., Flexural toughness of steel fiber reinforced concrete. *ACI Materials Journal*, **89** (1992) 541–546.
5. Jenq, Y. S. & Shah, S. P., Mixed-model fracture of concrete. *International Journal of Fracture*, **38** (1988) 123–142.
6. Li, V. & Liang, E., Fracture process in concrete and fiber reinforced cementitious composites. *J. Eng. Mech.*, **112** (1986) 566–586.
7. Hillerborg, A., Analysis of fracture by means of the fictitious crack model, particularly for fiber reinforced concrete. *The International Journal of Cement Composites*, **2** (1980) 177–184.
8. Swenson, D. V., & Ingraffea, A. R., The collapse of the schoharie creek bridge: a case study in concrete fracture mechanics. *International Journal of Fracture*, **51** (1991) 73–92.
9. Guinea, G. V., Planas, J. & Elices, M., Correlation between the softening and size effect curves. JCI International Workshop on Size Effect in Concrete Structures, Sendai, Japan, 31 October–2 November 1993, pp. 211–223.
10. Mai, Y. W., Fracture mechanics of cementitious composites. In *Application of Fracture Mechanics of*

Cementitious Composites, edited by S. P. Shah. Northwestern University, Evanston, Illinois, U.S.A., 1984, pp. 289–319.
11. Halvorsen, G. T., *J*-integral study of steel fiber reinforced concrete. *International Journal of Cement Composites*, **2** (1980) 35–420.
12. Mindess, S., Fracture Toughness Testing of Cement and Concrete, in *Fracture Mechanics of Concrete*. Martinus Nijhoff Publishers, 1984, pp. 67–110.
13. H.F. Büeckner, A novel principle for the computation of stress intensity factors. *ZAMM*, **50** (1970) 529–546.
14. J.R. Rice, Some remarks on elastic crack-tip stress fields. *Int. J. Solids Structures*, **8** (1972) 751–758.
15. Wu, X. R. & Carlsson, A. J., *Weight Functions and Stress Intensity Factor Solutions*. Pergamon Press, 1991.
16. H.J. Petroski & J.D. Achenbach, Computation of the weight function from a stress intensity factor. *Eng. Fracture Mech.*, **10** (1978) 257.
17. D.S. Dugdale, Yielding of steel sheets containing slits. *J. Mech. Phys. Solids*, **8** (1960) 100.
18. Barenblatt, G. J., The mathematical theory of equilibrium crack in the brittle fracture. *Advances in Applied Mechanics*, 7 (1962) 55–125.
19. Tada, H., Paris, P. & Irwin, G., *The Stress Analysis of Cracks Handbook*. Del Research Corporation, St. Louis, Missouri, 1973.
20. Eissa, Abou-Bakr H., Toughness measurements of high strength concrete reinforced with steel fibers. PhD Dissertation. Clarkson University, Potsdam, NY, 1994.
21. Swamy, R. N., Linear Elastic Fracture mechanics of concrete. In *Fracture Mechanics of Concrete*, edited by F. H. Wittman, Elsevier Science Publishers, Netherlands, 1983, pp. 411–461.
22. Americqan Society for Testing and Materials (ASTM), *Standard Method of Test for Flexural Toughtness of Fiber-Reinforced Concrete*, Vol. 04.02, C1018-92, pp. 510–516, August 1992.
23. Japan Society of Civil Engineers, Method of Tests for Steel Fiber Reinforced Concrete, Standard No. SF4 for Flexural Strength of SFRC, pp. 58–62. June 1984.